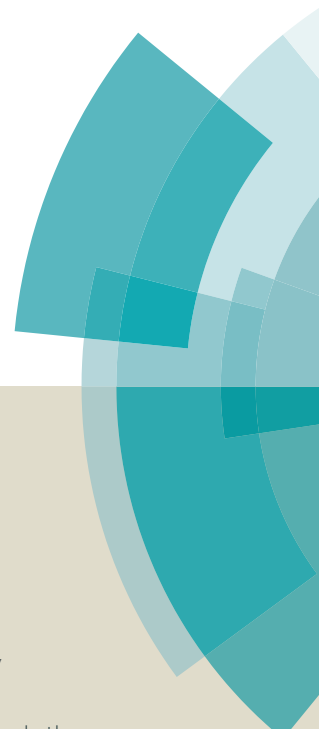
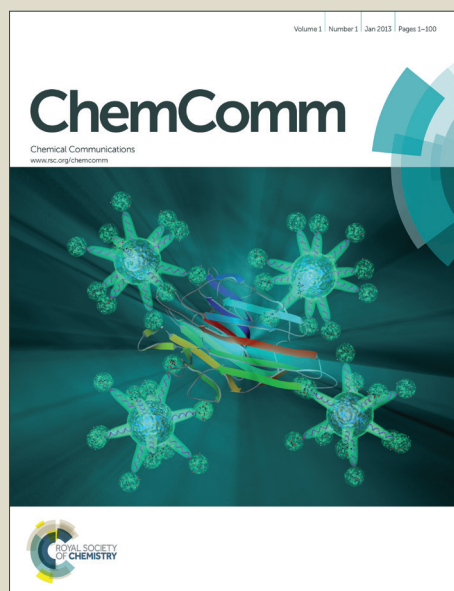


ChemComm

Accepted Manuscript



This article can be cited before page numbers have been issued, to do this please use: L. Wang, N. Lin, J. Zhou, Y. Zhu and Y. Qian, *Chem. Commun.*, 2014, DOI: 10.1039/C4CC09233C.



This is an *Accepted Manuscript*, which has been through the Royal Society of Chemistry peer review process and has been accepted for publication.

Accepted Manuscripts are published online shortly after acceptance, before technical editing, formatting and proof reading. Using this free service, authors can make their results available to the community, in citable form, before we publish the edited article. We will replace this *Accepted Manuscript* with the edited and formatted *Advance Article* as soon as it is available.

You can find more information about *Accepted Manuscripts* in the [Information for Authors](#).

Please note that technical editing may introduce minor changes to the text and/or graphics, which may alter content. The journal's standard [Terms & Conditions](#) and the [Ethical guidelines](#) still apply. In no event shall the Royal Society of Chemistry be held responsible for any errors or omissions in this *Accepted Manuscript* or any consequences arising from the use of any information it contains.

Cite this: DOI: 10.1039/C4CC09233C

www.rsc.org/xxxxxx

ARTICLE TYPE

Silicon nanoparticles obtained via a low temperature chemical “metathesis” synthesis route and its lithium-ion batteries property

Liangbiao Wang, Ning Lin, Jianbing Zhou, Yongchun Zhu,* and Yitai Qian*

Received (in XXX, XXX) Xth XXXXXXXXX 20XX, Accepted Xth XXXXXXXXX 20XX

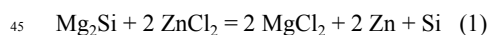
DOI: 10.1039/b000000x

Silicon (Si) nanoparticles have been prepared by a “metathesis” reaction of magnesium silicide (Mg₂Si) and zinc chloride (ZnCl₂) in an autoclave at 300 °C. The as-prepared Si nanoparticles exhibit a reversible capacity of 795 mA h g⁻¹ at a current density of 3.6 A g⁻¹ over 250 cycles.

Silicon (Si) materials have been widely used in the fabrication of solar cells, optical fibres, silicones, and Si chips.¹⁻² Recently, Si materials have been considered as a promising anode materials for lithium-ion batteries due to the high theoretical specific capacity (3579 mA h g⁻¹).³⁻⁵ Therefore, the production of Si materials has become the focus of research work due to their brilliant prospects.

Various methods have been developed to produce Si materials. Si materials have been synthesized by pyrolysis of Si organic compounds such as silanes or polysilanes.⁶⁻¹⁰ The carbothermic reduction and magnesiothermic reduction of silicon oxide have been applied to produce Si in industry.¹¹⁻¹³ SiCl₄ can also be reduced to prepare Si by various reductants (naphthalene sodium or sodium potassium alloy) in organic solvents.¹⁴⁻¹⁷ Recently, aqueous synthesis of Si nanoparticles under the microwave irradiation has been reported,¹⁸ our group has synthesized Si by hydrothermally reduction of silica sol or metasilicate nonahydrate.¹⁹⁻²⁰ Also, the metathesis reactions have been applied to synthesize materials, such as, reacting Mg₂Si together with SiCl₄,²¹ the Mg₂Si reduction of amorphous silica or silicon monoxide through high energy mechanical milling process,²²⁻²³ reacting “Zintl phases” (NaSi, KSi) together with metal halides or ammonium salts.²⁴⁻²⁷ Recently, the molten LiCl/KCl has been employed as the solvent for the synthesis of Si nanoparticles through the magnesiothermic reduction of SiO₂ at 550-800 °C.²⁸ Si materials have been synthesized by electro-deoxidation of SiO₂ in molten calcium chloride at 850 °C.²⁹⁻³⁰

Herein, crystalline silicon nanoparticles have been prepared by a “metathesis” reaction of magnesium silicide (Mg₂Si) and zinc chloride (ZnCl₂) in an autoclave at 300 °C. ZnCl₂ with melting point of 290 °C was chosen which not only acts as molten salt, but also participates in the reaction. The driving force for the reaction is provided by the formation of MgCl₂, together with metallic Zn and Si. The reaction can be described as follows:



As anode materials for lithium ion batteries, the as-prepared Si nanoparticles exhibit a reversible capacity of 795 mA h g⁻¹ at a current density of 3.6 A g⁻¹ over 250 cycles.

X-ray powder diffractions (XRD) analysis is used to determine the phases of the samples. Fig. 1a shows the XRD pattern of the sample without any treatment. The reflection peaks can be assigned to a mixture of Si (labeled as “◆” JCPDS 77-2111), MgCl₂ (labeled as “◇” JCPDS 25-1156) and Zn (labeled as “▼” JCPDS 04-0831). The other reflection peaks in Fig. 1a might come from the excess ZnCl₂. No reflection peaks of Mg₂Si can be identified in Fig. 1a, indicating that Mg₂Si has been completely transformed to Si and MgCl₂ under our experimental conditions. The XRD pattern of the sample after treatment with diluted HCl solution is displayed in Fig. 1b. All of the peaks in Fig. 1b can be indexed as cubic Si with calculated lattice constants $a = 5.433 \text{ \AA}$, which are very close to the reported data (JCPDS 77-2111). The XRD patterns offer the direct evidence that the method to synthesize Si proceeded according to the reaction (1).

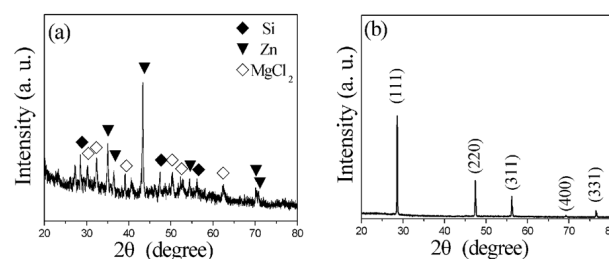


Fig. 1 (a) XRD pattern of the sample without any treatment. (b) XRD pattern of the same sample after the HCl treatment.

The morphology of the obtained sample is observed FESEM and TEM. The typical FESEM image (Fig. 2a) reveals that the sample consisted of nanoparticles. The TEM image further reveals the Si nanoparticles with diameters ranging from several tens of nanometers to 100 nm as shown in Fig. 2b. From the HRTEM image (Fig. 2c), the clearly resolved interplanar distances are all measured to be 0.19 nm, corresponding to the (220) and (202) crystal planes of the cubic Si. The separation angle between them is measured to be 60°. The typical SAED pattern of the Si nanoparticles (inset of Fig. 2c) can be indexed to the [111] zone axis of cubic Si. The EDX spectrum (Fig. 2d)

indicates that the sample consist of Si. The Cu signals are attributed to the Cu TEM grid that the samples are put on.

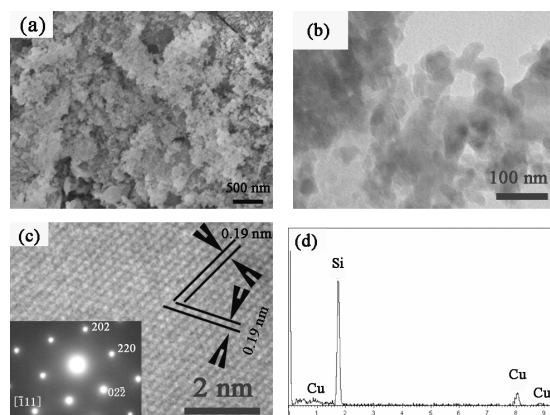


Fig.2 (a) FESEM image of the sample. (b) TEM image of the sample. (c) HRTEM image of the sample and SAED (inset). (d) EDX spectrum of the sample

Raman spectroscopy is utilized to understand the structure of the Si nanoparticles obtained by this metathesis reaction.³¹ It was reported that the transverse optical peak in Raman spectrum of bulk crystalline Si was usually observed at 520 cm^{-1} . The Raman spectrum of the as-prepared Si nanoparticles is shown in Fig. 3a. The sharp peak at 515 cm^{-1} is attributed to the Si–Si stretching mode in crystalline Si, which shifts to a lower frequency with broadened full width at half maximum due to the diameters' decrease. In addition, two broad peaks at 301 and 955 cm^{-1} observed in Fig.3a are assigned to the overtones of TA(X) and TO(L), respectively.³² The surface composition of the obtained Si nanoparticles is further examined by the XPS spectrum, as shown in Fig.3b. The peaks at 99.4 eV and 103.5 eV are assigned to Si⁰ and Si⁴⁺ of element, which indicates a small amount of silica are present in the as-prepared sample.³³

In this reaction system, ZnCl_2 as an oxidant can oxidize Mg_2Si to Si nanoparticles, meanwhile, molten ZnCl_2 (Melting point of ZnCl_2 is 290 °C) provides a high temperature stable liquid reaction medium which could increase the contact area between Mg_2Si and ZnCl_2 , facilitating the formation of crystalline Si at a low temperature. Based on the calculation of the free energy, equation (1) is thermodynamically spontaneous and highly exothermic ($\Delta_r G_m = -370.43$ kJ/mol, $\Delta_r H_m = -365.44$ kJ/mol). According to the $\Delta_r H_m$ value of equation (1), it is suggested that tremendous heat generated in the process urges the reaction to proceed continuously at the reaction temperature. When the reaction temperature is set to 250 °C (below the melting point of ZnCl_2), although equation (1) is thermodynamically spontaneous ($\Delta_r G_m = -369.83$ kJ/mol), crystalline Si can't be obtained which further proves that ZnCl_2 in the molten state is very important for synthesis of crystalline Si nanoparticles during the reaction. In the series of experiments have carried out in the reaction time range 4–20 h, we find that the yield of Si nanoparticles is very low when the reaction time is decreased to 4 h, and the yield of Si nanoparticles reaches a maximum of 80% when the reaction time

up to 10 h. The yield of the product was almost constant if the reaction time is more than 10 h.

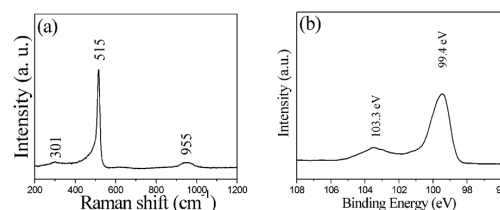


Fig.3 (a) Raman spectrum, (b) XPS spectrum of the sample.

To disclose the electrochemical properties of the prepared Si nanoparticles as anode for rechargeable lithium-ion batteries, a series of electrochemical tests are carried out. Fig.4a shows the discharge/charge voltage profiles of the Si electrode. The main discharge potential plateau is located at near 0.1 V (vs. Li/Li^+), which is assigned to the lithiation of crystalline Si and the formation of Li_xSi . The first discharge and charge capacity are of 3196 and 2169 mA h g^{-1} , respectively, corresponding to initial coulombic efficiency of 68%. The irreversible capacity of first cycle is normally caused by the inevitable formation of solid electrolyte interface (SEI) membrane and side reactions between bare Si nanoparticles and electrolyte (especially LiPF_6). In the subsequent cycles, the discharge potential plateau, around 0.1 V (vs. Li/Li^+) that occurred in the first cycle, is replaced by a group of sloping curves, mainly, resulted from the phase change of Si nanoparticles from crystallized to amorphous structure during the first lithiation/delithiation process. Notably, the 5th and 10th curves are overlapped well, indicating fine reversible reaction between lithium ion and Si electrode.

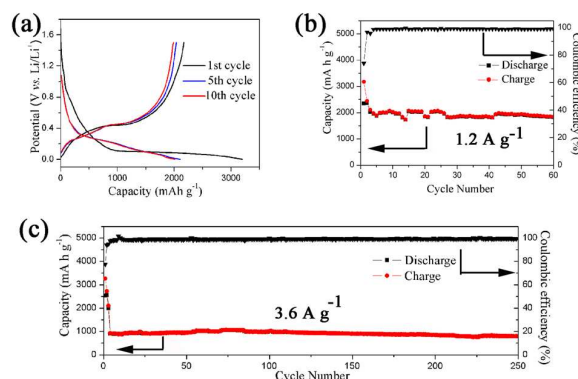


Fig.4 (a) Typical galvanostatic discharge-charge curves of the Si nanoparticles in the potential region of 0.005–1.5 V versus Li/Li^+ at a current density of 0.20 A g^{-1} of first cycle, and 0.4 A g^{-1} for the 5th and 10th cycles. Cycling property and coulombic efficiency of the Si nanoparticles at the current density of: (b) 1.2 A g^{-1} , (c) 3.6 A g^{-1} .

Furthermore, the cycling behavior of Si electrode is evaluated at different current densities by galvanostatic charge/discharge measurements. It should be mentioned that the first three cycles of the cells tested at a relative low current density of 0.2 A g^{-1} is to activate Si nanoparticles sufficiently. As can be seen in Fig.4b,

the Si anode exhibits capacity retention of 1822.8 mA h g⁻¹ at a current density of 1.2 A g⁻¹ after 60 cycles. The corresponding coulombic efficiency curve of Si shown in Fig.4b, the coulombic efficiency quickly increases from 74% of first cycle to 93.5 % of the second cycle and further reaches to over 98 % after several cycles, which is meaningful for practical application. As the current density increases to 3.6 A g⁻¹ (shown in Fig.4c), the Si anode delivers a specific capacity of 795.20 mA h g⁻¹ even over 250 cycles, which is over two times of traditional graphite anode (372 mA h g⁻¹). Remarkably, from the third to the 250 th cycles, almost 88% capacity retention is obtained, implying superior cycleability. When the active material density of the cell was increased to be 1.1 mg cm⁻², the Si anode exhibits capacity retention of 720 mA h g⁻¹ at a current density of 3.6 A g⁻¹ after 150 cycles.

The good electrochemical properties of the samples could be attributed to the nano-size particles of Si obtained in the designed reaction (1). The good electrochemical performance of the nano-size Si particles obtained in the designed reaction (1) with a synthesis route of chemical “metathesis” synthesis route could be attributed to the following aspects: First, the nano-size of the obtained Si provide void space to accommodate volume expansion during electrochemical cycles,³ and the existence of amorphous SiO₂ may effectively accommodate the volume changes. What is more, the obtained small primary nanoparticles of Si facilitates the ionic and electronic transfer over shorter distances.³⁴⁻³⁵ In addition, the uniformly dispersed nanoparticle structures supply more active sites for the contact between the electrode materials and electrolyte. It's all above aspects that affect the electrochemical performance of as obtained Si and enhance its lithium-storage capacity and stability of long cycling.

Conclusions

In summary, the molten salt route is an efficient and green method that can be applied in the preparation of different inorganic nanoparticles. The present work demonstrates that Si nanoparticles can be prepared by a chemical reaction of Mg₂Si and ZnCl₂ in an autoclave at 300°C. The method is based on the reaction of magnesium silicide and zinc chloride in the liquid environment of molten ZnCl₂. The obtained Si nanoparticles exhibit excellent lithium-storage capacity, high-rate capability and long cycling performance.

Experimental Section

Synthesis

The Mg₂Si was purchased from Johnson Matthey Company. All the other reagents used in the experiments were purchased from Shanghai Chemical Reagents Co. To prevent oxygen contamination, all manipulations were carried in a glove box purged with nitrogen gas. In a typical procedure, Mg₂Si (0.76 g) and ZnCl₂ (5.00 g) were loaded into a stainless steel autoclave of 20 mL capacity. The autoclave was sealed and heated in an electric stove with a heating ramp rate of 10 °C/min and maintained at 300 °C for 10 h, and then it was cooled to room temperature naturally. The followed detail treatment process can

be described as follows: The precipitate in the autoclave was collected and treated with dilute hydrochloric acid (1 mol/L) in a beaker of 250 mL capacity (The pH value of the solution is less than 1), which was stirred vigorously for 2 h and kept at room temperature for 8 hours. Then the result precipitate was washed with distilled water and ethanol for 3 times. The final sample was dried in vacuum at 50 °C for 10 h for further characterization.

Characterizations

XRD measurements were carried out with a Philips X'pert X-ray diffractometer (CuKα λ = 1.54178 Å). The scanning electron microscopy (SEM) images were taken by using a field-emission scanning electron microscope (FESEM, JEOL-JSM-6700F). The transmission electron microscopy (TEM) images, high-resolution transmission electron microscopy (HRTEM) images, the energy dispersive X-ray spectrometry (EDX) and the selected-area electron diffraction (SAED) patterns were taken on a JEOL-2010 transmission electron microscope with an accelerating voltage of 200 kV. Room-temperature Raman spectra were taken with a Spex 1403 Raman spectrometer, equipped with an Ar⁺ ion laser as a light source operating at a wavelength of 514.5 nm. X-ray photoelectron spectroscopy (XPS) was performed on an ESCA-Lab MKII X-ray photoelectron spectrometer, using Mg Kα X-ray as the excitation source.

Electrochemical measurements

The electrochemical properties of Si electrodes were measured with coin-type half cells (2016 R-type) which were assembled in an argon-filled glove box (H₂O, O₂ < 1 ppm). Metallic Li sheet was used as counter and reference electrode, and 1M LiPF₆ in a mixture of ethylene carbonate/dimethylcarbonate (EC/DMC; 1:1 by Volume) was used as the electrolyte (Zhuhai Smoothway Electronic Materials Co., Ltd (China)). For preparing working electrode, a slurry mixture of Si nanoparticles, super P carbon black, and sodium alginate (6:2:2 wt%) was pasted onto a Cu foil and then dried in a vacuum oven at 80 °C for 12 h. It is noted that the active material density of each cell was determined to be 0.5-1.0 mg cm⁻². Galvanostatic measurements were conducted using a LAND-CT2001A instrument at room temperature that was cycled between 0.005 V and 1.50 V (vs. Li⁺/Li). Cyclic voltammetry (CV) was performed on electrochemical workstation (CHI660D), with a scanning rate of 0.2 mV s⁻¹ at room temperature.

Acknowledgements

This work was supported by the 973 Project of China (No. 2011CB935901), the National Natural Science Fund of China (No. 91022033, 21201158)

Notes and references

Hefei National Laboratory for Physical Science at Micro-scale, Department of Chemistry, University of Science and Technology of China, Hefei, Anhui 230026, (P. R. China). E-mail: ychzhu@ustc.edu.cn; yqian@ustc.edu.cn

- 1 A. Shah, P. Torres, R. Tscharnner, N. Wyrsch and H. Keppner, *Science*, 1999, **285**, 692-698.
- 2 A. I. Hochbaum, R. Chen, R. D. Delgado, W. Liang, E. C. Garnett, M. Najarian, A. Majumdar and P. Yang, *Nature*, 2008, **451**, 163-167.
- 3 J. R. Szczech and S. Jin, *Energy Environ. Sci.*, 2011, **4**, 56-72.
- 4 L.-F. Cui, L. Hu, J. W. Choi and Y. Cui, *ACS Nano*, 2010, **4**, 3671-3678.
- 5 T. Hang, H. Nara, T. Yokoshima, T. Momma and T. Osaka, *J. Power Sources*, 2013, **222**, 503-509.
- 6 J. D. Holmes, K. P. Johnston, R. C. Doty and B. A. Korgel, *Science*, 2000, **287**, 1471-1473.
- 7 C. K. Chan, H. Peng, G. Liu, K. Wrath, X. F. Zhang, R. A. Huggins and Y. Cui, *Nat. Nanotechnol.*, 2008, **3**, 31-35.
- 8 K. Peng, Y. Yan, S. Gao and J. Zhu, *Adv. Mater.*, 2002, **14**, 1164-1167.
- 9 H. Okamoto, Y. Sugiyama and H. Nakano, *Chem. Eur. J.*, 2011, **17**, 9864-9887.
- 10 A. M. Morales and C. M. Lieber, *Science*, 1998, **279**, 208-211.
- 11 M. Nagamori, I. Malinsky and A. Claveau, *Metall. Trans. B*, 1986, **17**, 503-514.
- 12 Z. Bao, M. R. Weatherspoon, S. Shian, Y. Cai, P. D. Graham, S. M. Allan, G. Ahmad, M. B. Dickerson, B. C. Church, Z. Kang, H. W. Abernathy Iii, C. J. Summers, M. Liu and K. H. Sandhage, *Nature*, 2007, **446**, 172 - 175.
- 13 A. Xing, J. Zhang, Z. H. Bao, Y. F. Mei, A. S. Gordinc and K. H. Sandhage, *Chem. Comm.*, 2013, **60**, 6743-6745.
- 14 J. R. Heath, *Science*, 1992, **258**, 1131-1133.
- 15 F. Dai, J. T. Zai, R. Yi, M. L. Gordin, H. Sohn, S. R. Chen and D. H. Wang, *Nat. Commun.*, 2014, **5**, 3605-3615.
- 16 J. Zou, P. Sanelle, K. A. Pettigrew, and S. M. Kauzlarich, *J. Clust. Sci.*, 2006, **4**, 565-578.
- 17 N. Shirahata, T. Hasegawa, Y. Sakka and T. Tsuruoka, *Small*, 2010, **6**, 915-921.
- 18 Y. Zhong, F. Peng, F. Bao, S. Wang, X. Ji, L. Yang, Y. Su, S.-T. Lee, Y. He, *J. Am. Chem. Soc.* 2013, **135**, 8350-8356.
- 19 J. W. Liang, D. H. Wei, N. Lin, Y. C. Zhu, X. N. Li, J. J. Zhang, L. Fan and Y. T. Qian, *Chem. Commun.*, 2014, **50**, 6856-6859.
- 20 J. W. Liang, X. N. Li, Y. C. Zhu, C. Guo and Y. T. Qian, *Nano Res.*, DOI 10.1007/s12274-014-0633-6.
- 21 C. S. Yang, R. A. Bley, S. M. Kauzlarich, H. W. H. Lee and G. R. Delgado, *J. Am. Chem. Soc.*, 1999, **121**, 5191-5195.
- 22 Y. Hwa, W. -S. Kim, B. -C. Yu, J. -H. Kim, S. -H. Hong and H.-J. Sohn, *J. Power Sources*, 2014, **252**, 144-149.
- 23 R. Epur, L. Minardi, M. K.Datta, S. J. Chung and P. N. Kumta, *J. Solid State Chem.*, 2013, **208**, 93-98.
- 24 K. A. Pettigrew, Q. Liu, P. P. Power and S. M. Kauzlarich, *Chem. Mater.*, 2003, **15**, 4005-4011.
- 25 R. A. Bley and S. M. Kauzlarich, *J. Am. Chem. Soc.*, 1996, **118**, 12461-12462.
- 26 D. Neiner, H. W. Chiu and S. M. Kauzlarich, *J. Am. Chem. Soc.*, 2006, **128**, 11016-11017.
- 27 P. F. McMillan, J. Gryko, C. Bull, R. Arledge, A. J. Kenyon and B. A. Cressey, *J. Solid State Chem.*, 2005, **178**, 937-949.
- 28 X. F. Liu, C. Giordano and M. Antonietti, *J. Mater. Chem.*, 2012, **22**, 5454-5459.
- 29 X. B. Jin, P. Gao, D. H. Wang, X. H. Hu and G. Z. Chen, *Angew. Chem., Int. Ed.*, 2004, **43**, 733-736.
- 30 J. Zhao, J. Li, P. Ying, W. Zhang, L. Meng and C. Li, *Chem. Commun.*, 2013, **49**, 4477-4479.
- 31 R. P. Wang, G. W. Zhou, Y. L. Liu, S. H. Pan, H. Z. Zhang, D. P. Yu and Z. Zhang, *Phys. Rev. B: Condens. Matter*, 2000, **61**, 16827-16832.
- 32 X. H. Yu, F. H. Xue, H. Huang, C. J. Liu, J. Y. Yu, Y. J. Sun, X. L. Dong, G. Z. Cao and Y. G. Jung, *Nanoscale*, 2014, **6**, 6860-6865.
- 33 M. R. Alexander, R. Short, F. Jones, W. Michaeli and C. Blomfield, *Appl. Surface Sci.*, 1999, **137**, 179-183.
- 34 C. K. Chan, H. Peng, G. Liu, K. Wrath, X. F. Zhang, R. A. Huggins and Y. Cui, *Nat. Nanotechnol.*, 2008, **3**, 31-35.
- 35 N. Lin, J. B. Zhou, Y. C. Zhu and Y. T. Qian, *J. Mater. Chem.A*, 2014, **2**, 19604-19608.